Available online at www.sciencedirect.com
ScienceDirect
Journal of Power Sources 164 (2007) 659–667
JOURNAL OF POWER SOURCES
www.elsevier.com/locate/jpowsour

Effects of coal syngas and H_2S on the performance of solid oxide fuel cells Part 2. Stack tests

Andres I. Marquez [a,*], Ted R. Ohrn [b], Jason P. Trembly [a], David C. Ingram [d], David J. Bayless [c,1]

[a] 251 Stocker Center, Mechanical Engineering Department, Ohio University, Athens, OH 45701, United states
[b] SOFCo-EFS, Alliance, OH, United States
[c] 248 Stocker Center, Ohio University, Athens, OH 45701, United States.
[d] 106 Edwards Accelerator Laboratory, Department of Physics and Astronomy, Ohio University, Athens, OH 45701

Received 6 August 2006; received in revised form 20 October 2006; accepted 23 October 2006
Available online 14 December 2006

Abstract

The performance of two-cell planar solid oxide fuel cell stacks using coal syngas, with and without hydrogen sulfide (H_2S), was studied. All cells were tested at 850 °C with a constant current load of 15.2 A (current density of 0.22 A cm^{-2} per cell) and 30% fuel utilization. The H_2S injection immediately and significantly affected the power degradation of the stack system regardless of the carrier fuel. Results for the test with only H_2 and N_2 in the presence of H_2S (119–120 ppm) indicated that the power decay and area-specific resistance (ASR) degradation values were lower than those for the tests where simulated syngas containing CO and increased water content was used. The results indicate that contact points in the stack contributed to the power degradation of the system. Other factors, including contamination from the upstream fuel gas tubing, may have contributed to the higher degradation under simulated syngas conditions. In general the data confirm previous results for single cell testing, and showed that for this specific short stacks (two-cells) arrangement both a fast and a slow response to H_2S injection that eventually stabilized.

Keywords: Solid oxide fuel cell stacks; Sulfur tolerant anode; Coal syngas; Experimental performance; Long-term testing

1. Introduction

Solid oxide fuel cell (SOFC) technology has become a leading candidate for future coal-fueled power generation systems because it can use carbon monoxide (CO) in syngas [1–4]. However, most syngas fuels also contain hydrogen sulfide (H_2S), which presents a significant hurdle to implementing a syngas SOFC [1]. In addition, stacks of planar SOFCs in series need to be assembled to produce sufficient power for a variety of applications [5–12]. These stacks present many challenges, namely: materials cost and development, electrical conductivity between the materials (cells, interconnects) and their interfaces across the stack arrangement, and high temperature material degradation [3–5,7–30]. Several studies modeling planar SOFC stacks have been conducted to evaluate the performance of the stacks under a variety of conditions and situations [9,31–46]. Table 1 summarizes the main experimental and modeling studies involving planar stack SOFC testing. In summary, the literature indicates that the stability of the materials in a planar SOFC stack configuration has not been studied in depth or that the experiments have not been performed for long periods of time when using H_2S and/or syngas.

This paper reports the long-term performance of two-cell planar solid oxide fuel cell stacks (short stacks) in experiments with coal-derived syngas (H_2, CO and H_2O) with and without the presence of H_2S.

2. Experimental

2.1. Stack test setup

The electrolyte-supported planar solid oxide fuel cells used in these studies were provided by SOFCo-EFS. Briefly, they consist of a three-layered anode (a layer nickel and gadolinium

* Corresponding author. Tel.: +1 740 593 4916; fax: +1 740 593 0476.
E-mail addresses: marquez@ohio.edu (A.I. Marquez), trohrn@sofco-efs.com (T.R. Ohrn), bayless@ohio.edu (D.J. Bayless).
[1] Tel.: +1 740 331 4536.

0378-7753/$ – see front matter © 2006 Elsevier B.V. All rights reserved.
doi:10.1016/j.jpowsour.2006.10.102

Table 1
Summary of several studies of planar stack SOFC systems

Type of work/material under study	Conditions/details	Reference
Experimental/hermetic solid-state sealant between interconnect and electrolyte	Leak rate testing inside an alumina tube mounted on a furnace; ac impedance	[3]
Experimental/ScSZ-based anode and electrolyte materials	Natural gas reforming; 1000 °C; 1 kW SOFC system (68 cells stacks)	[4]
Experimental/all-ceramic interconnect material for SOFC; 10 kW SOFC system	Multilayer ceramic packaging; tape-casting, screen printing, co-sintering	[5,6,14,18,22,23]
Experimental/modeling/ceramic interface contact resistance	Applied mechanical load on LSM pellets; 1000 °C	[8]
Modeling/micro-thin film SOFCs	Effect on thin-film geometry on thermal stress and mechanical stability	[9]
Experimental/modeling/ceramic interface contact resistance	Auxiliary power unit applications; stack of 60 cells; 850 °C; fuel is CPOX diesel reformate	[11]
Experimental/novel interconnect material PrCaCrO	H_2 fuel; YSZ–SOFC; 800 °C	[12]
Experimental/La–Ga electrolyte material; 1 kW generator	Intermediate temperature SOFC (600–800 °C); natural gas fuel	[15]
Experimental/silver wire seal	Metallic interconnect; one-cell stack; leak rates; 500 °C	[16]
Experimental/LaCaCrO seal	Interlayer reactions; elemental diffusion; YSZ-CrO SOFC; 1200–1400 °C	[17]
Experimental/dynamic behavior of short stacks	H_2–air; 750–825 °C; five-cell stack; thermal cycling; ac impedance	[19]
Experimental/reactive air-brazing for hermetic sealing of SOFCs	Ni–YSZ, YSZ, metallic interconnect; sealing tests; thermal cycling	[20]
Experimental/alternate sealing materials for SOFCs stacks	Mica powers; metallic interconnects; leak rate tests; 800 °C	[25]
Experimental/metallic interconnect, Haynes 242 alloy	Ar–H_2–H_2O fuel; oxidation of Cr; Cr_2O_3 formation	[26]
Experimental/interactions steel interconnect—glass–ceramic sealants	YSZ, LSM/LSFC; 800 °C; Ar–H_2 fuel	[28]
Modeling/planar SOFC stacks	H_2 fuel; Ni–ZrO_2 anodes; 800 °C	[31]
Modeling/stack as network of hydraulic resistances	Gas distribution; manifold channels; H_2-water fuel; 800–1000 °C	[34,35]
Modeling/micro-structural optimization; anode supported SOFCs	H_2-water fuel/air; 600–800 °C; interconnect resistance, ohmic loss	[36]
Modeling/numerical study of SOFC stacks cell-to-cell variations	One-dimensional/co-flow model; CFD techniques	[38]
Modeling/novel design for SOFC stacks	Reduced spatial variations; H_2-water fuel/air	[39]
Modeling/three-dimensional electrochemical model for SOFC stacks	CFD techniques; co-flow; temperature distribution; PEN body	[41]
Modeling/mass and heat transport in planar substrates SOFCs	Two-dimensional; heat and mass transfer; porous substrates; CH_4 reforming	[46]

doped ceria [Ni-GDC], a layer of GDC and a layer of Ni); a tape cast 3 mol% yttria doped stabilized electrolyte; and a two-layers cathode: one of La0.75Sr0.2MnO3 (LSM) and 3YSZ and on top of that a layer of LSM only [1]. Further details about the construction of the cells have been provided in the literature [1]. Each stack was made of three ceramic interconnects, top and bottom current collector plates, and two planar 72.7 cm^2 cells (see Fig. 1). Sealant was added to prevent fuel leakage, while conductive vias provided the paths for the current to flow across the stacks. Air and fuel were provided to the stack assembly, and the internal manifolds of the interconnects provided fuel to the anode side and air to the cathode side, respectively (Figs. 2 and 3). The cathode and anode gas streams pass through the stack assembly in a co-flow arrangement (Figs. 2 and 3) [5,13,14,18,23]. The ceramic interconnect used in the stack arrangement was made of multiple layers of yttria-stabilized zirconia (YSZ) (Figs. 1 and 2) [5,13,14,18]. Two-cell short stacks were assembled and tested under syngas operation to examine performance and behavior of the components.

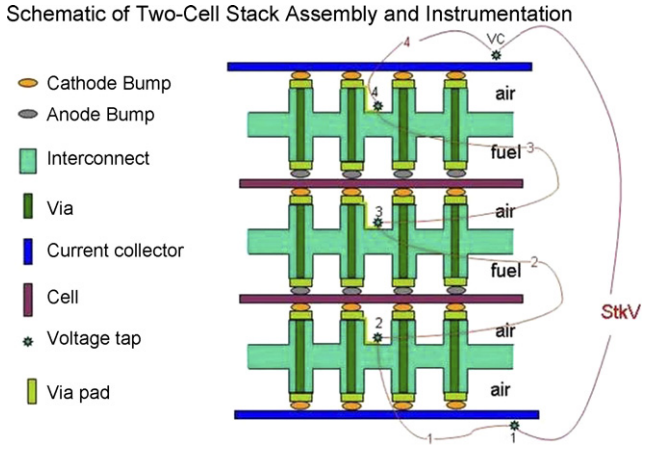

Fig. 1. Schematic of a short-stack (two-cell) assembly.

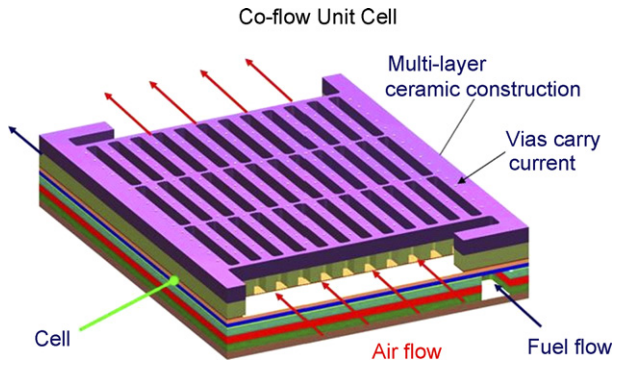

Fig. 2. The stack assembly, showing the co-flow fuel/air configuration and the interconnect structure with flow channels for air and fuel.

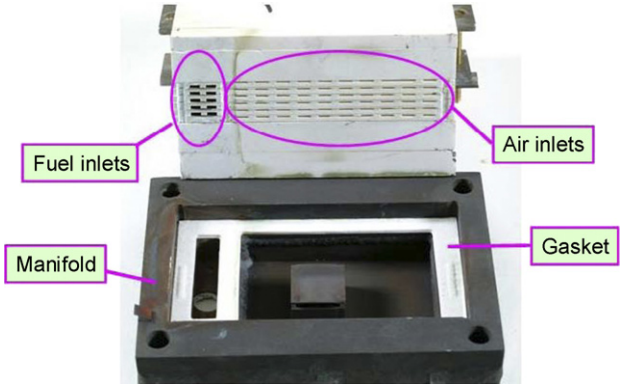

Fig. 3. Inlet manifold of a typical stack assembly.

The experimental setup for the stack tests is illustrated in Figs. 3 and 4. Similar to previous work at Ohio University [1], a gas delivery system (GDS) and a data acquisition system were used to carefully establish and monitor experimental conditions. The flow diagram and PID for the anode stream of the GDS is given in the previous reference [1]. The fuel stream consisted of a combination of H_2, N_2, CO, H_2O, and H_2S blended together in the desired composition using the GDS, as to simulated syngas conditions. The reactive fuel flow (H_2 and CO) was kept constant for all conditions at 0.75 slpm to maintain relatively constant fuel utilization (at 30%). The N_2 flow used was 0.75 splm for test with only H_2 and N_2, but was reduced to 0.38 slpm for simulated syngas tests. H_2S was introduced, from a small cylinder of pure H_2S, in the fuel stream system by using the GDS as to achieve a contaminant level of 119–120 ppm H_2S. Water was added to the fuel stream by passing the mixture through a water bubbler located at the test stand. Water temperature was varied from room temperature to 70 °C to control H_2O content. The airflow was held constant at 8.0 slpm for all experiments. For all the tests, the temperature was kept constant at 850 °C.

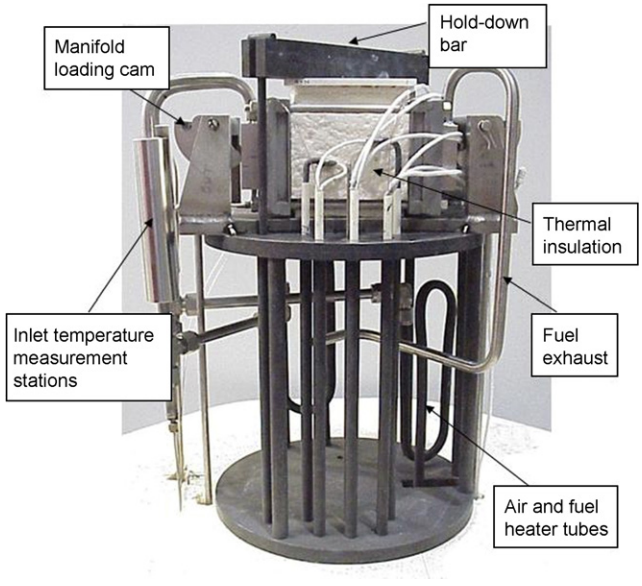

Fig. 4. The stack is installed inside the thermal insulation, shown near the center of the test stand.

2.2. Experimental testing

Tests were initially started using a fuel gas mixture of H_2/N_2 humidified to 3% H_2O. The start-up procedure was similar to previous work with the tests run under constant current control but with a slight increase in the operating current load to 15.2 A, or a current density of 0.22 A cm^{-2} for each of the 72.7 cm^{-2} cells [1]. Two primary fuel gas mixtures were used maintaining 30% fuel utilization. The first set of tests used equal parts of H_2 and N_2, while the second was a simulated syngas blend of H_2, CO, and N_2. In order to prevent carbon deposition additional water was added to the fuel gas by increasing the water bubbler temperature, thereby enlarging the steam to carbon ratio [1]. In both set of tests, H_2S was injected in a 119–120 ppm level as to evaluate its effect on the performance. Similar instrumentation for the electrochemical experiments, data acquisition and material analysis was used as in previous work, and all the experiments were completed at the SOFCo-Alliance facilities [1].

3. Results and discussion

3.1. Test with syngas mixture CO–H_2–N_2–H_2O

The performance of the stack voltage drops (Fig. 1) and current were measured for a representative test (Stack 3) under syngas conditions. Fig. 5 shows the stack power on a per cell basis for the test and also indicates the anode feed gas composition. The bubbler temperature indicates the fraction of water vapor in the anode gas. The test was started with a dry 50/50 H_2/N_2 mixture humidified with approximately 3% H_2O. After 45 h CO was introduced and the water fraction was increased to 30–31% by raising the bubbler temperature as shown in Fig. 5. The power dropped immediately after the CO/H_2O injection due to the change in Open Cell Voltage (OCV) and continued to decrease at a rate of about 30% per 500 h (see Table 2). After returning to H_2/N_2 conditions at 215 h, the power recuperated entirely, but only for a few hours, and then continued to decay at approximately 30% per 500 h. The power level degradation rate slowed near the end of the test. In total, the stack was exposed to syngas conditions for 170 h and the results clearly indicate that the simultaneous injection of CO and increased

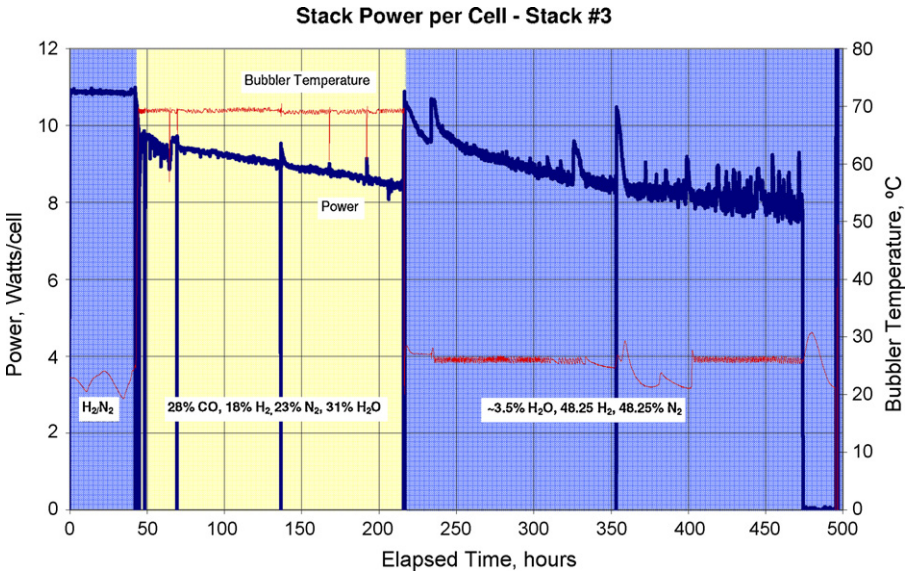

Fig. 5. Power and bubbler temperature traces for the test of Stack 3, running with syngas for about 170 h. The bubbler temperature was raised to 70 °C to ensure high water content (30–31% in the mixture), for 170 h to match the CO injection.

water content had a significant effect on the short stack power performance.

The ASR variation for this test is shown in Fig. 6. The stack started with an ASR of 1.40 Ω cm^2 per cell; with cell average values of 1.20–1.25 Ω cm^2 per cell (see Table 2). After 140 h, or almost 100 h under syngas conditions, the ASR degradation values of the stack and the cells increased to 1.60 Ω cm^2 and 1.40 Ω cm^2 per cell, respectively. After returning to initial fuel conditions, the ASR values continued to increase. They reached 2.20 Ω cm^2 per cell for the stack and 2.00 Ω cm^2 per cell for the cell average after 350 h (135 h on H_2/N_2 with 3% H_2O). By the end of the test (475 h or 260 h after re-establishing initial conditions), the ASR degradation slowed. Values were 2.30 Ω cm^2 per cell for the stack and 2.15–2.20 Ω cm^2 per cell for the cells (Table 2).

Table 2
Results of the power degradation and ASR per test

Test no.	% Power degradation (per 500 h)	ASR value (Ω cm^2 per cell)	Time (h)	Fig.
Stack 3	30%	–	45	5
	30%	–	215	5
		1.40	0	6
		1.60	140	6
		2.20	350	6
		2.30	475	6
Stack 4	5%	–	100	8
	10%	–	165	8
	10%	–	219	8
	12%	–	630	8
	22%	–	After 630	8
	23%	–	1000	8
		1.25	0	9
		1.92 Cell 1	1000	9
		3.26 Cell 2	1000	9
Stack 5	15%	–	100	11
	11%	–	100.1	11, 12
	8%	–	1000	11
		1.57	0	13, 14
		2.40	1000	13, 14

The power decay and ASR degradation rate for the stack tests was nearly double that seen in previous single-cell tests [1], indicating an effect not only in the cells but also in the additional components of the stack, where the simultaneous injection of CO and increased water content caused the system to degrade at a high rate. The stack performance indicated contact failures as evidenced by the noisy power signal that is seen in Fig. 5. This was also observed during *V–I* scans (voltage versus current) as shown in Fig. 7, when the power temporarily recovered after taking the stack down to OCV and back up to power.

Post-test examination revealed evidence of deposition of Nickel, likely removed from the stand piping, in the flow control passages of the interconnects. Deposits in these passages

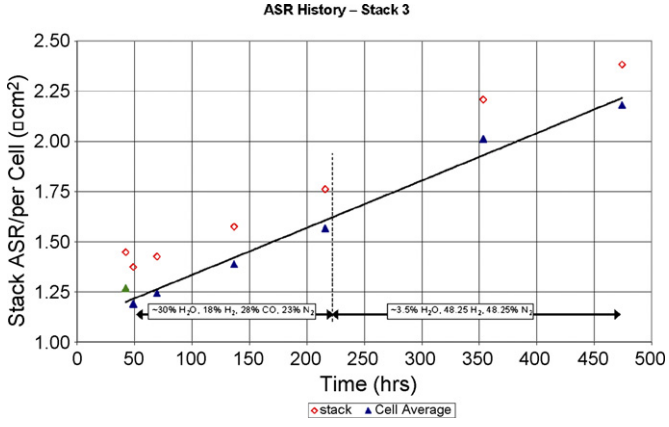

Fig. 6. ASR history for the test of Stack 3. The stack starts with an ASR of 1.40 Ω cm^2 per cell, with a cell average value of 1.20–1.25 Ω cm^2 per cell and increases over time. All the values of ASR are reported on a per cell basis (Ω cm^2 per cell).

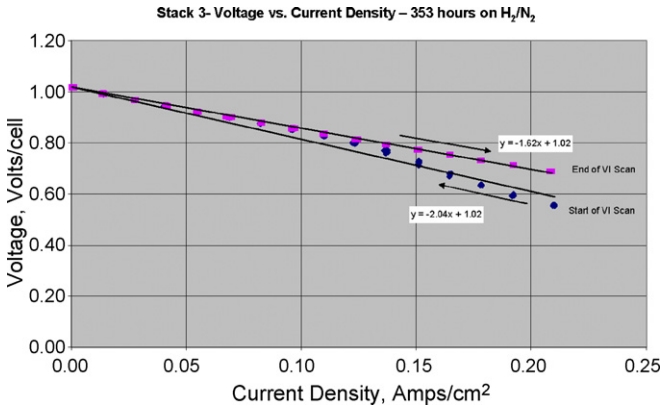

Fig. 7. *V–I* scan for Stack 3 taken 353 h after the start of test. The scan displays hysteresis as the power level reaches a higher value at the end of the scan than at the beginning.

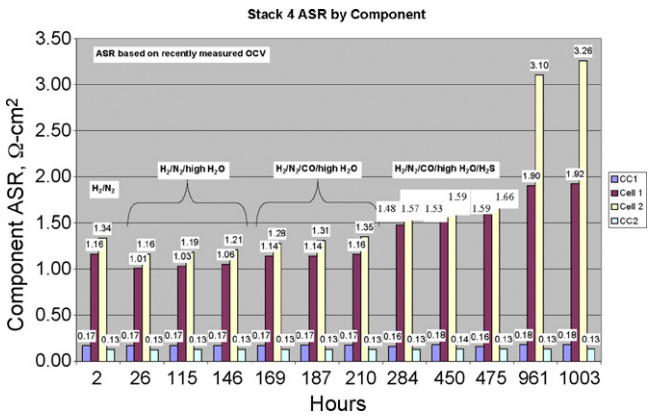

Fig. 9. History of individual stack contributions to the ASR based on measured OCV, for the test operating with syngas and H_2S (Stack 4). CC1 is Current Collector 1; CC2 is Current Collector 2; Cell 1 is the top cell in the stack schematic shown in Fig. 1. Cell 2 is the bottom cell. All the values of ASR are reported on a per cell basis ($\Omega\,cm^2$ per cell).

would increase the stack back pressure. Further, there was evidence of fuel leakage upstream of the stack at the inlet manifold, which could lead to fuel starvation of the cells and an increased degradation rate.

3.2. Test with syngas mixture and H_2S (119–120 ppm)

Fig. 8 displays the power trace for the test of Stack 4. The test was started with a 50/50 H_2/N_2 mixture humidified to approximately 3% H_2O. After 24 h of operation the bubbler temperature was raised to achieve 30–31% water content. The short stack was operated for 36 h under these conditions until the bubbler heater controller tripped off for 40 h as shown in Fig. 8. Increased bubbler temperature was re-established at 100 h and continued until 165 h, when CO was introduced to the stack. The data indicate that injection of CO caused the power decay rate to increase from about 5% for the H_2/N_2 operation up to more than 10% per 500 h (Table 2).

H_2S injection took place after 219 h and remained constant until 1000 h of operation. It had an immediate impact on power, which decreased approximately 10%, as shown in Fig. 8. The long-term degradation rate after the start of H_2S injection was relatively unchanged when compared to the trend after the start of CO injection and was about 12% per 500 h up to 630 h. At this time the degradation rate increased to about 22% per 500 h corresponding to an apparent change to Cell 2. The overall power degradation for the test was 23% per 500 h (Table 2).

Fig. 9 shows the individual contributions to the ASR (based on measured OCV) for each component shown in Fig. 1: bottom current collector (CC1), Cell 1, Cell 2, and top current collector (CC2). The contributions to ASR from the current collectors were essentially constant throughout the test. (The ASR for CC1 is larger than that of CC2 because it includes the bottom interconnect via resistance). The increase in ASR is observed in the two cell groups. Each group includes a cell, interconnects, and

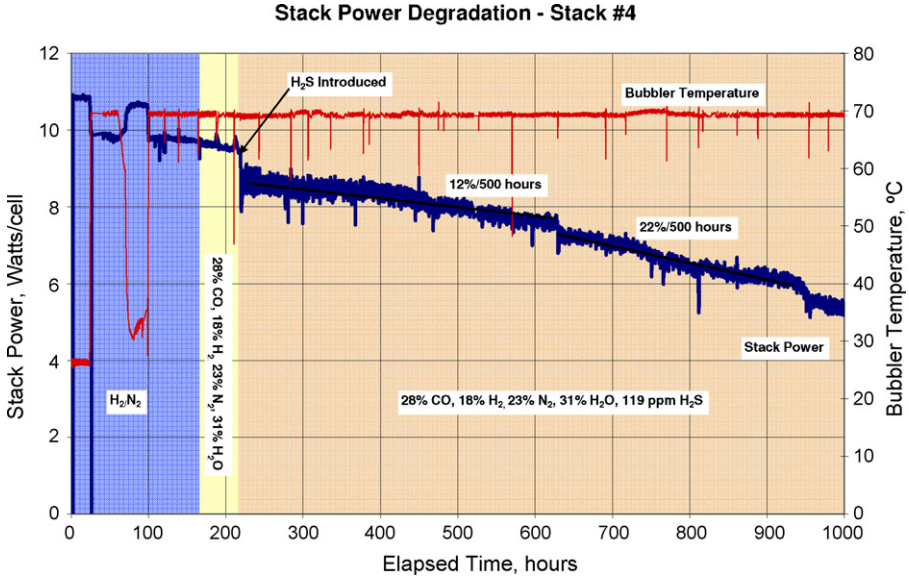

Fig. 8. Power and bubbler temperature history for the test of Stack 4, run with syngas and H_2S. CO was introduced after 165 h; H_2S was added after 219 h.

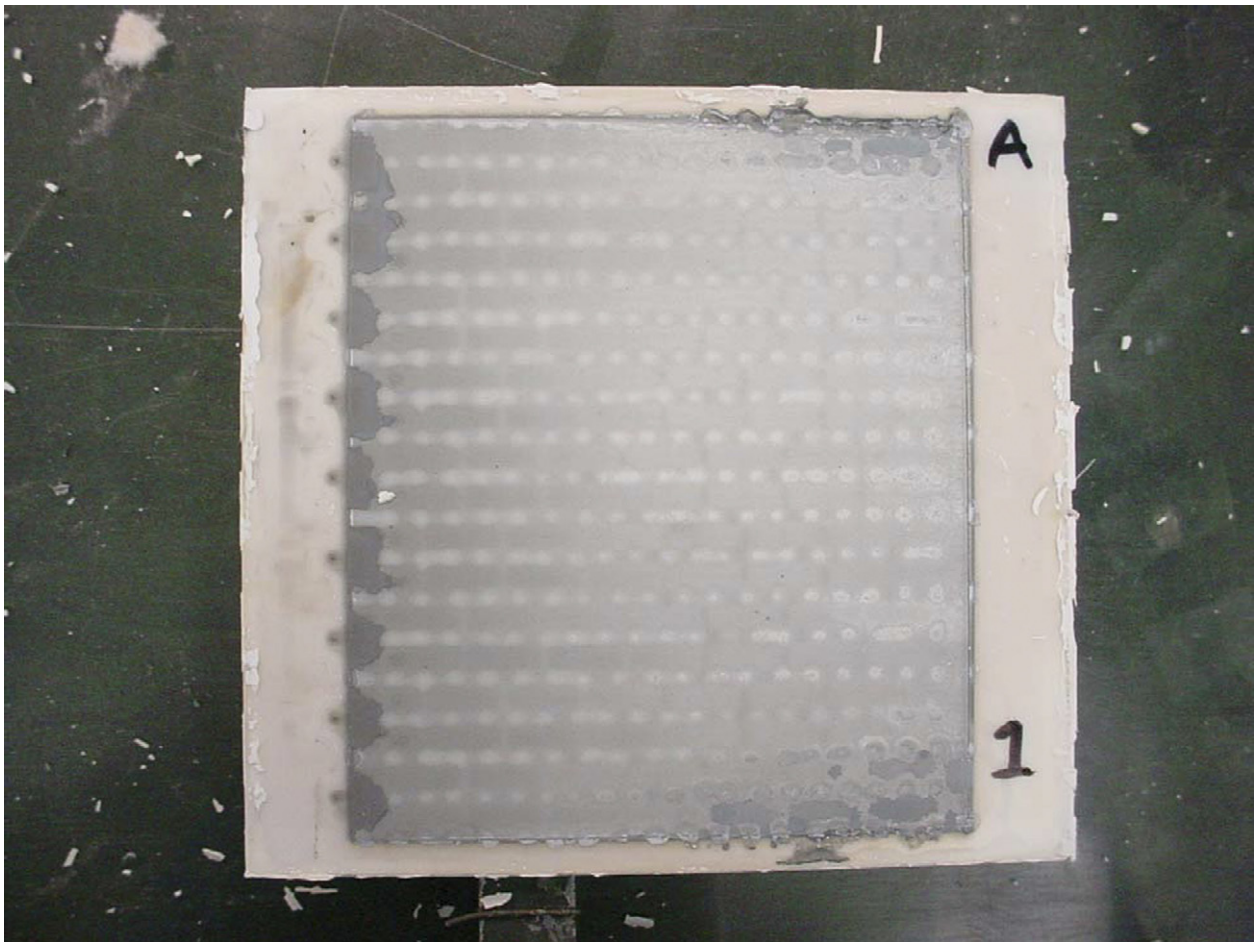

Fig. 10. Cell 1 after the test of Stack 4, showing the bond layer (conductive layer) on top of the anode nearly completely disbanded from the cell. The darker areas near left edge are the remaining bond layer.

contact resistances. Cell 2 (top cell, Fig. 1) showed a slightly higher ASR value than Cell 1 during the entire trial. The change in stack power after 630 h shown in Fig. 8 corresponds with the dramatic increase in the Cell 2 ASR. The average cell ASR based on measured OCV starts at 1.25 Ω cm^2 per cell with a final value of 1.92 Ω cm^2 per cell for Cell 1 and 3.26 Ω cm^2 per cell for Cell 2 (Table 2).

The anode side of the stack experienced increasing back pressure throughout the test and post-test examination again revealed deposition in the flow control passages of the interconnects as observed in Stack 3. The contacts between the cells and interconnects also may have contributed to the high degradation of the stack. During examination after testing, the bond layers on the anode side detached from the cells during disassembly, as shown in Fig. 10. This is unusual and is normally only seen in more localized regions. This was not observed in Stack 3 and may indicate an effect of the H_2S on the fuel stream.

3.3. Test with H_2 and H_2S (119–120 ppm)

For this test (Stack 5), the effects of only H_2S on the short stack were evaluated. The wet gas compositions were: 48.2% H_2, 48.2% N_2, and 3.6% H_2O. H_2S was injected after 100 h for an additional 900 h. The results are presented in Figs. 11–13. The initial power decay rate was approximately 15% per 500 h for the first 100 h of operation before the H_2S injection, as shown in Fig. 11. Within 30 min after H_2S was injected at 100.1 h, the average power decreased from 10.4 W to 9.5 W per cell, as shown in Fig. 12. The power then continued to decrease, and tends to level off to the baseline line degradation rate with having only H_2/N_2 (Stack 3 test, after 200 h in Fig. 5) at about 8% per 500 h as seen in Fig. 11. The total power degradation rate was about 11% per 500 h (Table 2). This strongly indicates that H_2S significantly affected the performance of the stack system.

Fig. 13 shows the ASR contribution history (based on measured OCV) for each component of Stack 5, which can be compared with Fig. 9 for Stack 4. Again, the contribution to the ASR from the current collectors remained essentially unchanged during the entire 1000 h of operation. From Fig. 13, the stack average ASR per cell based on measured OCV started at 1.57 Ω cm^2 per cell with a final value of 2.40 Ω cm^2 per cell (Table 2). Comparing these results to those of the Stack 4 test, the contributions of the cells to the stack degradation performance are significant, and the rate of degradation is lower than for the test combining higher water content, CO injection and H_2S injection.

The stack performance indicated contact failures as evidenced by the noisy power signal noted in Fig. 11. The *V–I* scans

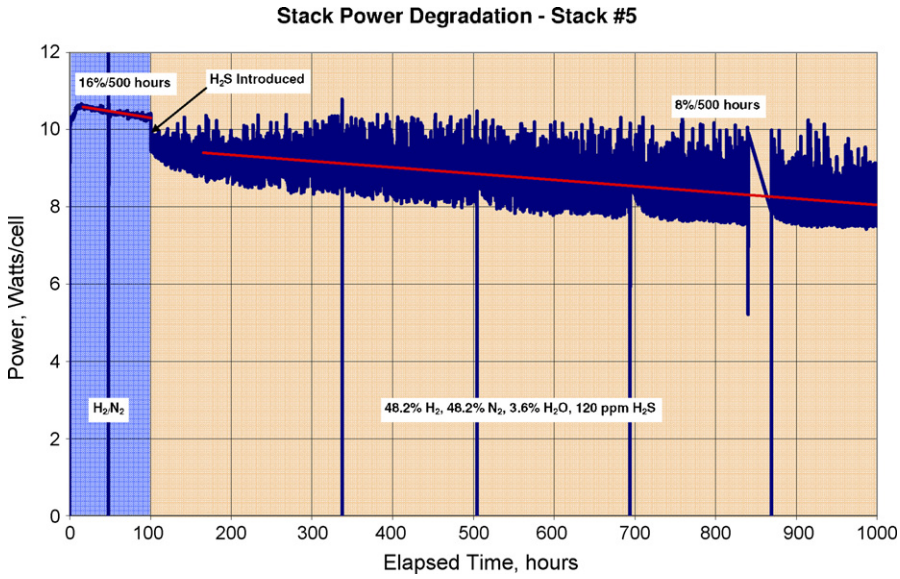

Fig. 11. Power trace for the test of Stack 5, run with only H_2/N_2 and H_2S. After 100 h, H_2S was introduced (119–120 ppm) and was kept constant until the conclusion of the test at 1000 h.

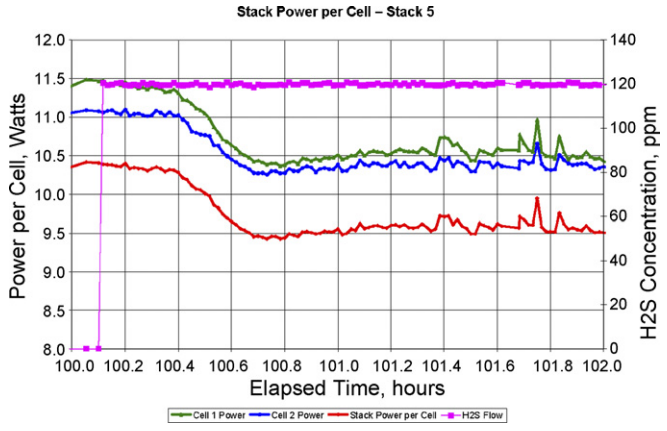

Fig. 12. Instantaneous power variation of each cell and the cell average for the test of Stack 5 after 100 h of operation (immediately after H_2S injection).

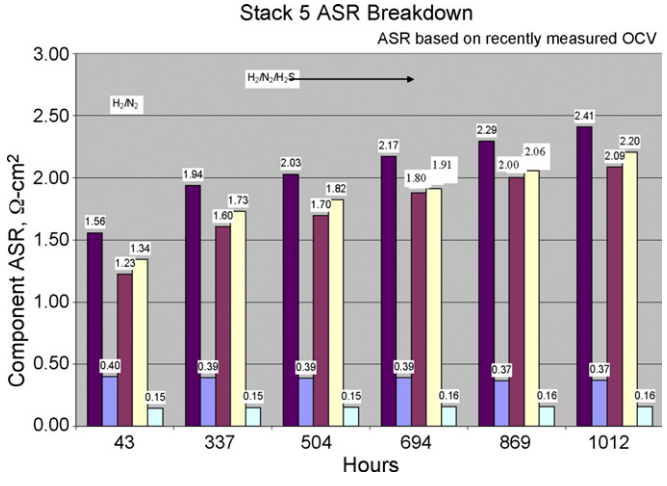

Fig. 13. History of individual stack contributions to the ASR, based on measured OCV, for the test operated with only H_2 and H_2S (Stack 5). All the values of ASR are reported on a per cell basis ($\Omega\,cm^2$ per cell).

in Fig. 14 show that before H_2S was injected, the ascending and descending *V–I* scan curves were very similar. However, the scan taken after 700 h of H_2S injection displays a hysteresis between the two curves, similar to that shown in Fig. 7 for Stack 3.

The data indicate that the average power decay when only H_2 and H_2S were present in the fuel mixture was half of the decay

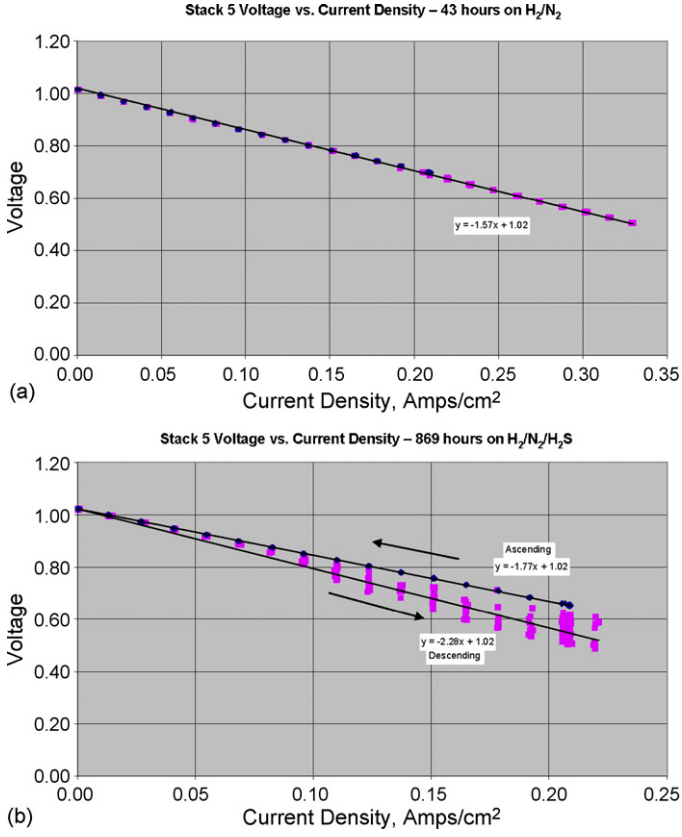

Fig. 14. *V–I* scans for the test of Stack 5: (a) after 43 h (beginning of the run); (b) near the end of the test (869 h).

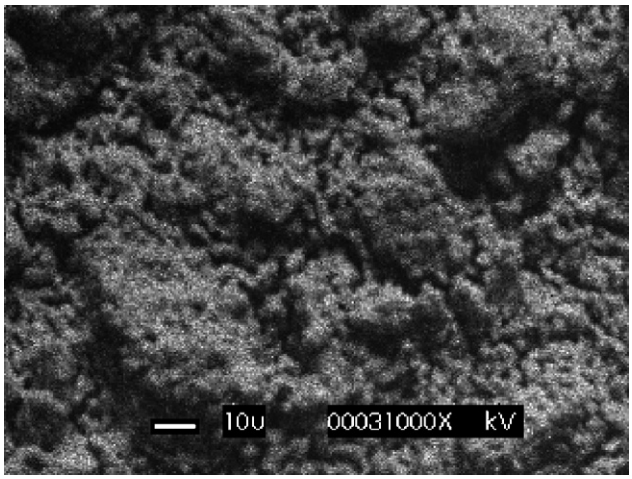

Fig. 15. SEM surface structure (top view) of a portion of the anode of an SOFC before testing.

when using syngas and H_2S. Therefore, even though H_2S was the main individual contributor to performance degradation, the combined effects of increased water content, CO injection and H_2S injection caused a higher degradation rate.

Post-test analysis revealed two notable findings. First there was no evidence of deposition in the interconnect flow control passages for Stack 5 as there was for Stacks 3 and 4. Secondly, the bond layers on the cell were intact for Stack 5 unlike Stack 4. The lack of deposition may indicate that the increased degradation for the high CO and H_2O fraction tests was related to a fuel starvation issue and not to a reaction with the cell or stack materials themselves.

3.4. Material analysis

A simplified analysis of the anode materials of each cell was performed using SEM and XPS characterization techniques to clarify individual cell contributions to the stack performance degradation. Fig. 15 shows the anode structure of a fresh cell. Fig. 16 shows the anode structure of a cell after more than 1000 h

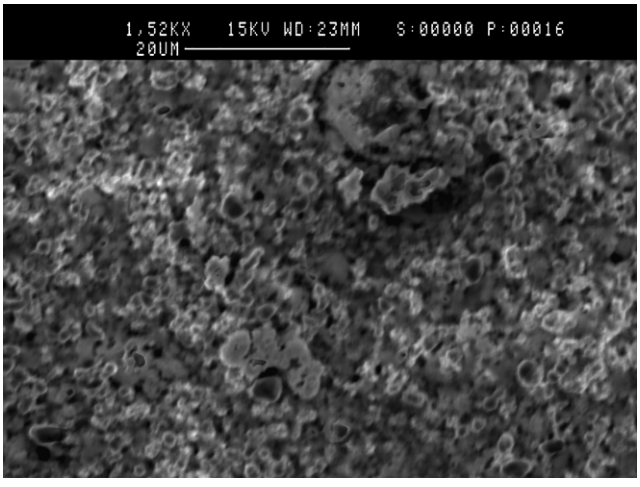

Fig. 16. SEM surface structure (top view) of a portion of the anode of an SOFC from Stack 5 after more than 1000 h of operation with only H_2 and H_2S.

of testing in Stack 5, which used only H_2 and H_2S. It was evident that the surface morphology of the cell tested with H_2 and H_2S significantly differed from that of the fresh cell, indicating that the H_2S diminished performance of the system, as previously found [1].

XPS analysis was performed on the anode materials before and after testing, which as mentioned before were similar to the previous work [1]. It was found that for the test with syngas operation (475 h total operation time, Stack 3), there was a slight loss of nickel at the surface of the anode material (1–3%), while the gadolinium doped ceria (GDC) gain was 3–4% and the loss of Ce was approximately 15–17%.

The anode material from Stack 4, tested with syngas and H_2S, had a loss of 7–9% nickel, a loss of 1–3% cerium, and a gain of 2–3% GDC. In addition, 1.5–2.0% sulfur was present.

Finally, the anode from Stack 5, tested with only H_2 and H_2S, had a nickel reduction of 4–6%, a cerium reduction of 12–14%, and a GDC gain of 2–3%. As in Stack 4 and in previous work, 1.5–2.0% sulfur was present [1].

These results suggest that while the GDC and Ce content changed for each test in a coupled fashion, the Ni and Ce mass concentration (%) given from the XPS analysis was always lowered due to the fuel oxidation preference on these two sites (Ni and Ce metals). Also, for the tests with H_2S, the Ni and Ce reductions suggest that the proposed mechanism for degradation may include NiS and CeS_2 formation at the surface of each cell. Further analysis of other components of the stack system is needed to verify this conclusion. As in previous work by Ohio University, other metals such as Fe, Cr, and Mo were also noticeable in all the tests, but their presence was due to the piping material (Inconel) used for the anode line, and they did not seem to affect the behavior of the cells [1]. Thus, the Ni-GDC cell still seems to be a candidate for operating with syngas in the presence of H_2S [1].

4. Conclusions

This work studied the effects of coal syngas, with and without H_2S, on the performance of short-stack planar solid oxide fuel cell assemblies. The results indicate that the separate effects of water content, CO, and H_2S can have significant deleterious effects on the long-term stack performance. The mechanism by which CO and high H_2O fraction affected stack performance was uncertain, and may be due to deposition in flow control passages of the interconnects. Such deposits could lead to increased back pressure on the stack and potentially more fuel leakage at the upstream manifold, making less fuel available for the stack.

The introduction of 119–120 ppm of H_2S caused an immediate power decay of approximately 10%. Tests with syngas and H_2S had an average final power decay rate per 500 h of 23%; almost double that for tests with only H_2 and H_2S (12%). Stack electrical contacts are suspected to be failing in these tests as evidenced by noisy power behavior and hysteresis in the *V–I* curves.

The results of the material analysis suggest that the presence of GDC improved the sulfur tolerance of the individual cells, but other components of the stack system require more analysis.

Acknowledgments

This work was supported by the U.S. Department of Energy (award no. DE-FG36-03GO13059). The authors would like to thank to Dick P. Glasser at SOFCo-EFS; Shyler Switzer, Patrick Curran and Micah McCreery at the Ohio University Coal Research Center for their collaboration in designing and assembling the GDS; Dr. Yolanda DeAbreu of Ohio University for assistance with the SEM images; and Dr. Iain Miller at Ohio University's Biosciences department for use of the SEM facilities.

References

[1] J.P. Trembly, A.I. Marquez, T.R. Ohrn, D.J. Bayless, J. Power Sources 158 (2006) 263–273.
[2] A.I. Marquez, Y. DeAbreu, G.G. Botte, Electrochem. Solid-State Lett. 9 (2006) A163–A166.
[3] C. Compson, M. Liu, Solid State Ionics 177 (2006) 367–375.
[4] Y. Mizutani, K. Hisada, K. Ukai, H. Sumi, M. Yokoyama, Y. Nakamura, O. Yamamoto, J. Alloys Compd. 408–412 (2006) 518–524.
[5] T.A. Morris, E.A. Barringer, S.C. Kung, R.W. Mckain, Mater. Res. Soc. Bull. 30 (2005) 596–600.
[6] D. Norrick, E. Barringer, M. Kantak, D. Sanders, G. Watson, SOFCo-EFS Holdings LLC, 2002.
[7] C. Barthet, F. Blein, J. Delepine, L. Lefebvre-Joud, CLEFS CEA 44 (2000–2001) 57–65.
[8] S. Koch, P.V. Hendricksen, Solid State Ionics 168 (2004) 1–11.
[9] Y. Tang, K. Stanley, J. Wu, D. Ghosh, J. Zhang, J. Micromech. Microeng. 15 (2005) S185–S192.
[10] K.E. Kneidel, C. DeBellis, M. Kantak, D. Norrick, C. Vesely, B.K. Palmer, SOFCo-EFS Holdings LLC, 2004.
[11] M. Stelter, A. Reinert, B.E. Mai, M. Kuznecov, J. Power Sources 154 (2006) 448–455.
[12] Z. Liu, D. Dong, X. Huang, Z. Lu, Y. Sui, X. Wang, J. Miao, X. Shen, W. Su, Electrochem. Solid-State Lett. 8 (2005) A250–A252.
[13] E.A. Barringer, K.E. Kneidel, T.A. Morris, T.L. Cable, Proceedings of the 2002 Fuel Cell Seminar, Palm Springs, CA, November 18–21, 2002.
[14] L.A. Xue, E.A. Barringer, T.L. Cable, R.W. Goettler, K.E. Kneidel, Int. J. Appl. Ceram. Technol. 1 (2004) 16–22.
[15] T. Inagaki, F. Nishiwaki, J. Kanou, S. Yamasaki, K. Hosoi, T. Miyazawa, M. Yamada, N. Komada, J. Alloys Compd. 408–412 (2006) 512–517.
[16] J. Duquette, A. Petric, J. Power Sources 137 (2004) 71–75.
[17] Y.-K. Lee, J.-W. Park, Mater. Chem. Phys. 45 (1996) 97–102.
[18] R. Goettler, T.L. Cable, K.E. Kdneidel, T.A. Morris, E.A. Barringer, SOFCo-EFS Holdings LLC, 2003.
[19] M. Molinelli, D. Larrain, N. Autissier, R. Ihringer, J. Sfeir, N. Badel, O. Bucheli, J.V. herle, J. Power Sources 154 (2006) 394–403.
[20] K.S. Weil, J.-Y. Kim, J.S. Hardy, Electrochem. Solid-State Lett. 8 (2005) A133–A136.
[21] K. Yasumoto, H. Itoh, T. Yamamoto, Proceedings of the Annual Electrochemical Society Conference, 2003.
[22] S. Elangovan, J.J. Hartvigsen, S.C. Kung, R.W. Goetler, E.A. Barringer, SOFCo-EFS Holdings LLC, 2001.
[23] Z. Liu, E. Barringer, R. Goettler, SOFCo-EFS Holdings LLC, 2004.
[24] W. Li, K. Hasinka, M. Seabaugh, S. Swartz, J. Lannutti, J. Power Sources 138 (2004) 145–155.
[25] M. Bram, S. Reckers, P. Drinovac, J. Monch, R.W. Steinbrech, H.P. Buchkremer, D. Stover, J. Power Sources 138 (2004) 111–119.
[26] S.J. Geng, J.H. Zhu, Z.G. Lu, Electrochem. Solid-State Lett. 9 (2006) A211–A214.
[27] H. Apfel, M. Rzepka, H. Tu, U. Stimming, J. Power Sources 154 (2006) 370–378.
[28] P. Batfalsky, V.A.C. Haanappel, J. Malzbender, N.H. Menzler, V. Shemet, I.C. Vinke, R.W. Steinbrech, J. Power Sources 155 (2006) 128–137.
[29] B.C.H. Steele, Solid State Ionics 134 (2000) 3–20.
[30] S. Elangovan, J. Hartvigsen, T.L. Cable, T.A. Morris, E.A. Barringer, Proceedings of the 2000 Fuel Cell Seminar, Portland, OR, October 30–November 2, 2000.
[31] J. Van-herle, D. Larrain, N. Autissier, Z. Wuillemin, M. Molinelli, D. Favrat, J. Eur. Ceram. Soc. 25 (2005) 2627–2632.
[32] A. Khandkar, J. Hartvigsen, S. Elangovan, Proceedings of the Sixth National Symposium on SOFCs, Honolulu, Hawaii, 1999.
[33] A. Khandkar, J. Hartvigsen, S. Elangovan, Proceedings of the Third European Solid Oxide Fuel Cell Forum, Nantes, France, June 2–5, 1998.
[34] R.J. Boersma, N.M. Sammes, J. Power Sources 66 (1997) 41–45.
[35] R.J. Boersma, N.M. Sammes, J. Power Sources 63 (1996) 215–219.
[36] D.H. Jeon, J.H. Nam, C.-J. Kim, J. Electrochem. Soc. 153 (2006) A406–A417.
[37] Y. Lu, L. Schaefer, J. Power Sources 153 (2006) 68–75.
[38] A.C. Burt, I.B. Celik, R.S. Gemmen, A.V. Smirnov, J. Power Sources 126 (2004) 76–87.
[39] A.M. Al-Qattan, D.J. Chmielewski, S. Al-Hallaj, J.R. Selman, Chem. Eng. Sci. 59 (2004) 131–137.
[40] Y. Shiratori, Y. Yamazaki, J. Power Sources 114 (2003) 80–87.
[41] K.P. Recknagle, R.E. Williford, L.A. Chick, D.R. Rector, M.A. Khaleel, J. Power Sources 113 (2003) 109–114.
[42] M. Roos, E. Batawi, U. Harnisch, T. Hocker, J. Power Sources 118 (2003) 86–95.
[43] A. Selimovic, J. Palsson, J. Power Sources 106 (2002) 76–82.
[44] W. Winkler, J. Power Sources 86 (2000) 449–454.
[45] H. Karoliussen, K. Nisancioglu, A. Solheim, J. Appl. Electrochem. 28 (1998) 283–288.
[46] T. Ackmann, L.G.J. de-Haart, W. Lehnert, D. Stolten, J. Electrochem. Soc. 150 (2003) A783–A789.